Spherical Wave Theory of Moiré Fringes Produced under Conditions of Borrmann Transmission by Two Crystals Separated by a Gap

S. Tanemura and A. R. Lang

H. H. Wills Physics Laboratory, University of Bristol, England

(Z. Naturforsch. **28 a**, 668–676 [1973]; received 14 February 1973)

Dedicated to Prof. Dr. G. Borrmann on his 65th birthday

The spherical wave theory of Kato is applied to calculate the intensity field in the moiré fringe pattern produced by two perfectly aligned simultaneously reflecting crystals separated by a gap when only anomalously transmitted waves need be taken into account. Under practical experimental conditions the incident wavefront curvature adds significantly to the phase difference between interfering waves. This contribution, together with a previously omitted term involving the ratio of gap width to sum of the crystal thicknesses, should be added to the argument of the trigonometric interference term used by previous workers in deriving structure factors from gap-fringe spacings. Expressed directly in terms of a change in the 220 structure factor, use of our revised interference term would reduce Hart and Milne's measured value for silicon by $\frac{1}{2}\%$ and Baker, Hart and Hel-liar's measured value for germanium by 1.3%.

1. Introduction

The type of X-ray moiré fringe patterns shown in Fig. 1 may be observed in diffracted-beam section topographs obtained under the diffraction geometry shown in Figure 2. They become dominant in the section topograph image when both crystals A and B are sufficiently perfect and thick, and the structure factor favourable, so that substantially only those rays are transmitted which have undergone Borrmann transmission in both A and B. These patterns might have remained a scientific curiosity but for their ingenious exploitation by Hart and co-workers [1, 2] as a new means for the absolute measurement of structure factors. It was, however, their moiré characteristics that were first studied. Following the observation of X-ray moiré fringes in the X-ray topographic images of cracks in plates of quartz [3], attempts were made to propagate cracks in quartz and silicon in a controlled way for the purpose of studying X-ray moiré patterns. This aim was eventually achieved with quartz [4], but in the case of silicon it was found easier to simulate a crack by making a fine saw-cut in a relatively thick crystal. A thick crystal was used both in order to simplify the diffraction problem by reducing the diffracted rays to only those that had belonged to branch (1) Bloch waves in both crystals, but also to keep the ratio of gap-width to total crystal thickness low so as to minimise the perturbation of the moiré pattern through presence of a gap between diffracting elements. The gap has the effect of adding a dilation component to the moiré pattern. Thus, in undistorted crystals, the fringes run per-

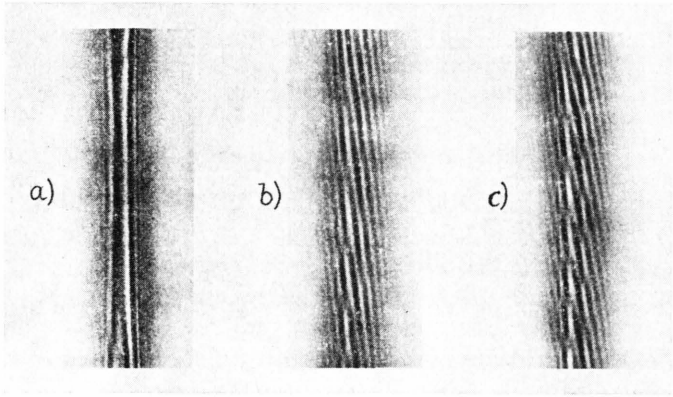

Fig. 1. Gap fringes with a twist-moiré component: (a) torque applied to annual intrinsic twist, (b) intrinsic twist only, the specimen being in its initial condition, (c) torque applied with opposite sense as in (a). Silicon, 220 reflection, MoKα_1 radiation, $t_A + t_B \approx 3.5$ mm, $t_g \approx \frac{1}{4}$ mm, gap-fringe spacing $\approx 130\ \mu$m.

Reprints requests to Dr. A. R. Lang, H. H. Wills Physics Laboratory, University of Bristol, Tyndall Avenue, Royal Fort, *Bristol* BS 8 1 TL, England.

pendicularly to the plane of incident and diffracted rays. Figure 1 records an early experiment performed by Milne and one of the authors (A. R. L.). After the gap was cut part of the way through a block of silicon single crystal, distortion resulting either from the relief of grown-in stresses or from the specimen preparation process caused the gap-fringe pattern to appear sloping, i. e. to have a twist-moiré component, as shown in Figure 1 (b). However, the crystal had been cut in such a way that by application of a small torque diffracting element B could be rotated relative to A about an axis normal to the plane of the gap without introducing other, unwanted distortions. Figure 1 (a) shows the annulment of the intrinsic twist by the application of such a torque, and Fig. 1 (c) shows an increase of the twist component of the moiré pattern by application of a torque of the opposite sense. There are several ways of regarding this pattern: the optical analogue of identical but separated gratings [6] may be used, for example. However, conventional X-ray dynamical theory will account for the pattern satisfactorily by considering the resultant amplitude at the exit face of B due to superposition of Bloch waves generated in B. Spherical wave theory must be used, of course, but its implications need carefuly examining. Such an examination is here presented. The spherical wave treatment as published by Authier et al. [7] does not display the moiré character of gap-fringes. Our stricter treatment does so. Moreover, we find among the factors that need to be considered when attempting precise analysis [1, 2] of gap fringe patterns one of fundamental nature that has escaped attention: the effect of incident wavefront curvature.

2. Theory

2.1. The Component Plane Waves

Before performing the integrations required by the spherical wave theory we will set down the expressions for the component plane waves by whose coherent superposition the spherical waves may be represented. The geometry in real space is shown in Fig. 2 and in reciprocal space in Figure 3. It will be assumed that the four crystal surfaces (entrance and exit surfaces of the first crystal A and entrance and exit surfaces of the second crystal B) are all parallel. Figures 2 and 3 are drawn showing symmetrical Laue case transmission, for simplicity; but the expressions given in Sects. 2.1 and 2.2 are not limited to this case: specialisation to the symmetrical Laue case will be deferred until Section 2.3.

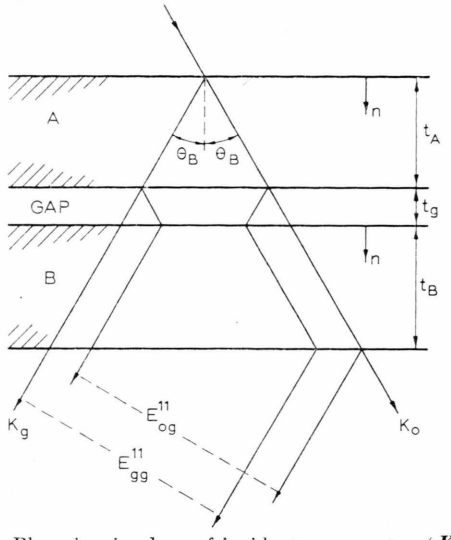

Fig. 2. Plan view in plane of incident wave vector ($\boldsymbol{K}_0$) and diffracted wave vector ($\boldsymbol{K}_g$) showing diffraction geometry with the sequence first crystal A, gap, and second crystal B. Drawn for symmetrical Laue case.

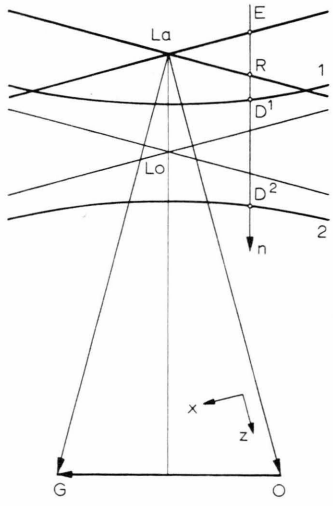

Fig. 3. Diagram in reciprocal space showing orientation of rectangular coordinate system employed: the y-axis is directed perpendicularly into the plane of the diagram. (For simplicity, the dispersion surfaces corresponding to only one polarisation mode are drawn.) The Laue point is L_a, the Lorentz point is L_0, the normal to the crystal surfaces is $\boldsymbol{n}$ (as in Figure 1). $\overrightarrow{L_a 0} = \overline{\boldsymbol{K}}_0$, $\overrightarrow{L_a G} = \overline{\boldsymbol{K}}_g$, and $|\boldsymbol{K}_g| = |\boldsymbol{K}_0| = K = 2\pi\lambda^{-1}$. $\overrightarrow{E\,0} = \boldsymbol{K}_e$, $\overrightarrow{R\,G} = \boldsymbol{K}_g$, $\boldsymbol{k}_0{}^i = \overrightarrow{D^i\,0}$, $\boldsymbol{k}_g{}^i = \overrightarrow{D^i\,G}$, $E\,D^1 = K\,\delta_e{}^1$, $E\,D^2 = K\,\delta_e{}^2$, $R\,D^1 = K\,\delta_g{}^1$, $R\,D^2 = K\,\delta_g{}^2$. [Note that the positive sign of the radical in Eq. (3 a) in the text corresponds to branch (1).]

Assume an incident plane wave represented by $E_e \exp\{i\,\boldsymbol{K}_e \cdot \boldsymbol{r}\}$. Solution of the boundary condi-

tions at entrance and exit faces of crystals A and B produces waves leaving crystal B in the diffracted beam direction which may be divided into the wave field $E_{0g}(\boldsymbol{r})$ arising from the waves travelling along the O-direction in the gap and which (for each polarisation state) consists of four component waves, and the wave field $E_{gg}(\boldsymbol{r})$ arising from waves travelling along the G-direction in the gap and which also consists of four component waves. Expressions for these wave fields are respectively

$$E_{0g}(\boldsymbol{r}) = E_{0g} \exp\{i\,\boldsymbol{K}_g \cdot \boldsymbol{r}\}\,, \tag{1 a}$$

with

$$E_{0g} = E_e \sum_{i=1}^{2} \sum_{j=1}^{2} C_{0g}^{ij} \exp\{i[(\boldsymbol{K}_e - \boldsymbol{k}_0{}^i) \cdot (\boldsymbol{r}_A - \boldsymbol{r}_{A'}) + (\boldsymbol{K}_e - \boldsymbol{k}_0{}^j) \cdot \boldsymbol{r}_B - (\boldsymbol{K}_g - \boldsymbol{k}_g{}^j) \cdot \boldsymbol{r}_{B'}]\} \tag{1 b}$$

and

$$E_{gg}(\boldsymbol{r}) = E_{gg} \exp\{i\,\boldsymbol{K}_g \cdot \boldsymbol{r}\} \tag{1 c}$$

with

$$E_{gg} = E_e \sum_{i=1}^{2} \sum_{j=1}^{2} C_{gg}^{ij} \exp\{i[(\boldsymbol{K}_e - \boldsymbol{k}_0{}^i) \cdot \boldsymbol{r}_A - (\boldsymbol{K}_g - \boldsymbol{k}_g{}^i) \cdot \boldsymbol{r}_{A'} + (\boldsymbol{K}_g - \boldsymbol{k}_g{}^j) \cdot (\boldsymbol{r}_B - \boldsymbol{r}_{B'})]\}. \tag{1 d}$$

The entrance and exit surfaces of crystal A are described by the position vectors $\boldsymbol{r}_A$ and $\boldsymbol{r}_{A'}$, and the entrance and exit surfaces of B correspondingly by $\boldsymbol{r}_B$ and $\boldsymbol{r}_{B'}$. The amplitude factors C_{0g}^{ij} and C_{gg}^{ij} are exactly as given by Kato, Usami and Katagawa [8]: the symbol C_{0g}^{ij}, for example, means the amplitude of the wave that has passed through crystal A in the state $\binom{i}{0}$ and in crystal B in the state $\binom{j}{g}$. Note that the C_{0g}^{ij} explicitly include the phase factor

$$\delta_{BA} = -2\pi\,\boldsymbol{g} \cdot \boldsymbol{d}$$

arising from a translation of crystal B relative to crystal A by the vector $\boldsymbol{d}$. The crystal wave vectors $\boldsymbol{k}_0{}^i$ and $\boldsymbol{k}_g{}^i = \boldsymbol{k}_0{}^i + 2\pi\,\boldsymbol{g}$ are related to the incident wave vector $\boldsymbol{K}_e$ and the external diffracted wave $\boldsymbol{K}_g$ as explained in Figure 3. In the equations

$$\boldsymbol{k}_0{}^i = \boldsymbol{K}_e - K\,\delta_e{}^i\,\boldsymbol{n} \tag{2 a}$$

and

$$\boldsymbol{K}_g = \boldsymbol{k}_g{}^i + K\,\delta_g{}^i\,\boldsymbol{n}\,, \tag{2 b}$$

the Anpassungen $K\,\delta_0{}^i$ and $K\,\delta_g{}^i$ are given by

$$K\,\delta_e{}^i = -K\,\chi_0/\gamma_0 - \alpha(s \pm \sqrt{s^2+\beta^2}) \tag{3 a}$$

and

$$K\,\delta_g{}^i = K\,\delta_e{}^i - K_x \sin 2\,\Theta_B/\gamma_g\,. \tag{3 b}$$

The rectangular coordinate system for wave vector components is oriented as shown in Figure 3; this, and the notation used in Eqs. (3 a,b), and subsequently, are the same as in the earlier works cited [8–10]. The deviation parameter employed, s, is given by

$$s = -K_x + (K\,\chi_0/2 \sin 2\,\Theta_B)\,(1 - \gamma_g/\gamma_0) \tag{4}$$

with

$$\beta = K\,C\,(\chi_g\,\chi_{\bar{g}})^{\frac{1}{2}}\,(\gamma_g/\gamma_0)^{\frac{1}{2}}\,\mathrm{cosec}\,2\,\Theta_B\,, \tag{5}$$

and K_x being the x-component of $\boldsymbol{K}_e$. The ratio α is $(\sin 2\,\Theta_B)/2\,\gamma_g$. Quantities familiar are the polarisation factor C ($=1$ or $|\cos 2\,\Theta_B|$), the cosines $\gamma_0 = (\bar{\boldsymbol{K}}_0 \cdot \boldsymbol{n})/|\bar{\boldsymbol{K}}_0|$ and $\gamma_g = (\boldsymbol{K}_g \cdot \boldsymbol{n})/|\boldsymbol{K}_g|$, $b = \gamma_0/\gamma_g$, and χ_i, the Fourier coefficients of order i of the polarisability of the crystal for X-rays.

Attention will be confined to situations when the only appreciable waves reaching the observation point (i. e. the photographic plate) are those that have undergone Borrmann transmission in both crystals. Through Eqs. (3) and (4) substitution for the amplitudes C_{0g}^{11} and C_{gg}^{11} can be made. The following expressions are obtained for the waves $E_{0g}^{11}(\boldsymbol{r})$ and $E_{gg}^{11}(\boldsymbol{r})$ at the observation point $\boldsymbol{r}$ (whose rectangular coordinates are referred to axes parallel to those shown in Fig. 3 but with origin in real space at the source point of the incident spherical wave):

$$E_{0g}^{11}(\boldsymbol{r}) = \tfrac{1}{4}\,E_e\,\beta\,(\chi_g/\chi_{\bar{g}})^{\frac{1}{2}}\,b^{\frac{1}{2}} \exp\{2\pi i\,\boldsymbol{g} \cdot \boldsymbol{r}\} \exp\{i\,\delta_{BA}\} \times \exp\{i(K_y y + K_z z)\} \exp i\{\tfrac{1}{2}\,K\,\chi_0[t\,\gamma_0{}^{-1} + (1-b^{-1})\,x\,\mathrm{cosec}\,2\,\Theta_B - (1-b^{-1})\,r'\,\gamma_g{}^{-1}]\} \times \left((-s + \sqrt{s^2+\beta^2})/(s^2+\beta^2)\right) \exp i\{[-x + \alpha(t+2r')]\,s + \alpha\,t\,\sqrt{s^2+\beta^2}\} \tag{6 a}$$

and

$$E_{gg}^{11}(\boldsymbol{r}) = \tfrac{1}{4}\,E_e\,\beta\,(\chi_g/\chi_{\bar{g}})^{\frac{1}{2}}\,b^{\frac{1}{2}} \exp\{2\pi i\,\boldsymbol{g} \cdot \boldsymbol{r}\} \times \exp\{i(K_y y + K_z z)\} \exp i\{\tfrac{1}{2}\,K\,\chi_0[t\,\gamma_0{}^{-1} + (1-b^{-1})\,x\,\mathrm{cosec}\,2\,\Theta_B - (1-b^{-1})\,(r'+t_g)\,\gamma_g{}^{-1}]\} \times \left((s + \sqrt{s^2+\beta^2})/(s^2+\beta^2)\right) \exp i\{[-x + \alpha(t+2r'+2t_g)]\,s + \alpha\,t\,\sqrt{s^2+\beta^2}\}\,. \tag{6 b}$$

In the above equations the substitutions $t_A + t_B = t$, and $r' = (\boldsymbol{r} - \boldsymbol{r}_{B'}) \cdot \boldsymbol{n}$, have been made.

2.2. *The Spherical Wave Solution*

The incident spherical wave can be represented by a Fourier integral as [9]

$$E_e\,\Phi = E_e[\exp\{i\,\boldsymbol{K} \cdot \boldsymbol{r}\}/4\pi r] = E_e(i/8\pi^2) \iint [\exp\{i\,\boldsymbol{K} \cdot \boldsymbol{r}\}/K_z]\,\mathrm{d}K_y\,\mathrm{d}K_z\,. \tag{7}$$

The spherical waves excited by $E_e\,\Phi$ which correspond to $E_{0g}^{11}(\boldsymbol{r})$ and $E_{gg}^{11}(\boldsymbol{r})$ are respectively

$$\Phi_{0g}^{11}(\boldsymbol{r}) = (i/8\pi^2)\iint (E_{0g}^{11}(\boldsymbol{r})/K_z)\,\mathrm{d}K_y\,\mathrm{d}K_z \tag{8a}$$

and

$$\Phi_{gg}^{11}(\boldsymbol{r}) = (i/8\pi^2)\iint (E_{gg}^{11}(\boldsymbol{r})/K_z)\,\mathrm{d}K_y\,\mathrm{d}K_z\,. \tag{8b}$$

Integration with respect to $\mathrm{d}K_y$ is carried out by the stationary phase method and results in the same multiplying factor

$$D_y = (2\pi K/z)^{\frac{1}{2}}\exp\{-\pi i/4\}$$

for both equations. Then Eqs. (8a) and (8b) may be rewritten as

$$\begin{aligned}\Phi_{0g}^{11}(\boldsymbol{r}) = {} & (i/32\pi^2)\,E_e\,\beta(\chi_g/\chi_{\bar{g}})^{\frac{1}{2}}\,b^{\frac{1}{2}}(2\pi/Kz)^{\frac{1}{2}}\exp\{2\pi i\,\boldsymbol{g}\cdot\boldsymbol{r}\}\exp\{i\,\delta_{BA}\}\\ & \times\exp\{i(Kz-\pi/4)\}\exp i\{\tfrac{1}{2}K\chi_0[t\gamma_0^{-1}+(1-b^{-1})\,x\,\mathrm{cosec}\,2\Theta_B-(1-b^{-1})\,r'\gamma_g^{-1}]\}\\ & \times\int_{-\infty}^{\infty}\left((-s+\sqrt{s^2+\beta^2})/(s^2+\beta^2)\right)\exp i\{[-x+a(t+2r')]\,s+a\,t\sqrt{s^2+\beta^2}\}\,\mathrm{d}s\end{aligned} \tag{9a}$$

and

$$\begin{aligned}\Phi_{gg}^{11}(\boldsymbol{r}) = {} & (i/32\pi^2)\,E_e\,\beta(\chi_g/\chi_{\bar{g}})^{\frac{1}{2}}\,b^{\frac{1}{2}}(2\pi/Kz)^{\frac{1}{2}}\exp\{2\pi i\,\boldsymbol{g}\cdot\boldsymbol{r}\}\\ & \times\exp\{i(Kz-\pi/4)\}\exp i\{\tfrac{1}{2}K\chi_0[t\gamma_0^{-1}+(1-b^{-1})\,x\,\mathrm{cosec}\,2\Theta_B-(1-b^{-1})\,(r'+t_g)\,\gamma_g^{-1}]\}\\ & \times\int_{-\infty}^{+\infty}\left((s+\sqrt{s^2+\beta^2})/(s^2+\beta^2)\right)\exp i\{[-x+a(t+2r'+2t_g)]\,s+a\,t\sqrt{s^2+\beta^2}\}\,\mathrm{d}s\,.\end{aligned} \tag{9b}$$

Now with usual experimental arrangements the distance from the exit face of crystal B to the photographic plate will be small compared with the distance from the X-ray source to the crystals. It will also be fairly small absolutely, say of order 1 cm. Under these conditions the wave fields $\Phi_{0g}^{11}(\boldsymbol{r})$ and $\Phi_{gg}^{11}(\boldsymbol{r})$ are described with sufficient precision as the wave fields at the exit face of crystal B. Expressing this approximation formally, we specify the arbitrary position vectors $\boldsymbol{r}_{B'}(^{11}_{0g})$ and $\boldsymbol{r}_{B'}(^{11}_{gg})$ which define the exit face of crystal B so that both $(\boldsymbol{r}-\boldsymbol{r}_{B'}(^{11}_{0g}))$ and $(\boldsymbol{r}-\boldsymbol{r}_{B'}(^{11}_{gg}))$ are parallel to $\boldsymbol{K}_g$. Then Eqs. (9a) and (9b) become

$$\Phi_{0g}^{11}(\boldsymbol{r}) = \exp\{i\,K\,L_{0g}\}\,\Phi_{0g}^{11}(\boldsymbol{r}_{B'}(^{11}_{0g})) \tag{9c}$$

and

$$\Phi_{gg}^{11}(\boldsymbol{r}) = \exp\{i\,K\,L_{gg}\}\,\Phi_{gg}^{11}(\boldsymbol{r}_{B'}(^{11}_{gg}))\,, \tag{9d}$$

in which $L_{0g} = |\boldsymbol{r}-\boldsymbol{r}_{B'}(^{11}_{0g})|$ and $L_{gg} = |\boldsymbol{r}-\boldsymbol{r}_{B'}(^{11}_{gg})|$;

and, by our definition, $L_{0g} = L_{gg}$. To evaluate the wave fields on the right hand sides of Eqs. (9c) and (9d), integration of Eqs. (9a) and (9b) is performed with $r' = 0$; and it is carried out by the stationary phase method. Finally there are obtained

$$\begin{aligned}\Phi_{0g}^{11}(\boldsymbol{r}_{B'}) = {} & (i/16\pi)\,E_e(\chi_g/\chi_{\bar{g}})^{\frac{1}{2}}\,(\beta/Kz_{B'})^{\frac{1}{2}}\exp\{2\pi i\,\boldsymbol{g}\cdot\boldsymbol{r}_{B'}\}\exp\{i\,\delta_{BA}\}\\ & \times\exp i\{\tfrac{1}{2}K\chi_0[t\gamma_0^{-1}+(1-b^{-1})\,x_{B'}\,\mathrm{cosec}\,2\Theta_B]+Kz_{B'}-\pi/4\}\\ & \times(\eta_1-\eta_2)/\eta_1\cdot 1/(\eta_1^2-\eta_2^2)^{\frac{1}{4}}\exp\{i[\beta\sqrt{\eta_1^2-\eta_2^2}+\pi/4]\}\end{aligned} \tag{10a}$$

and

$$\begin{aligned}\Phi_{gg}^{11}(\boldsymbol{r}_{B'}) = {} & (i/16\pi)\,E_e(\chi_g/\chi_{\bar{g}})^{\frac{1}{2}}\,(\beta/Kz_{B'})^{\frac{1}{2}}\exp\{2\pi i\,\boldsymbol{g}\cdot\boldsymbol{r}_{B'}\}\\ & \times\exp i\{\tfrac{1}{2}K\chi_0[t\gamma_0^{-1}+(1-b^{-1})\,x_{B'}\,\mathrm{cosec}\,2\Theta_B-(1-b^{-1})\,t_g\gamma_g^{-1}]+Kz_{B'}-\pi/4\}\\ & \times(\eta_1-\eta_3)/\eta_1\cdot 1/(\eta_1^2-\eta_3^2)^{\frac{1}{4}}\exp\{i[\beta\sqrt{\eta_1^2-\eta_3^2}+\pi/4]\}\,,\end{aligned} \tag{10b}$$

in which $\eta_1 = a\,t$, $\eta_2 = x_{B'}-a\,t$, and $\eta_3 = x_{B'}-a(t+2t_g)$.

As shown in Figs. 4a and 4b, $\eta_1+\eta_2$ and $(\eta_1-\eta_2)\,b^{-1}$ are the perpendicular distances from the position $\boldsymbol{r}'_B$ (denoted by the point S) to the lines O_1T_1 and O_1R_1 respectively. Correspondingly, $\eta_1+\eta_3$ and $(\eta_1-\eta_3)\,b^{-1}$ are the perpendicular distances from r'_B to O_2T_2 and O_2R_2. As Eqs. (10a) and (10b) show, the wave field of Φ_{0g}^{11} is restricted to the range $0 \leqq x_{B'} \leqq 2\,a\,t$ and Φ_{gg}^{11} is restricted to the range $2\,a\,t_g \leqq x_{B'} \leqq 2\,a(t+t_g)$.

2.3. The Intensity Field

From the above account we see that the wave fields under discussion are superimposed in the range of $x_{B'}$ given by $2\,a\,t_g \leqq x_{B'} \leqq 2\,a\,t$, i. e. the range R_1T_2 on the exit surface of crystal B (see Figure 4). In

order to simplify the expressions for the intensity field, we shall assume the symmetrical Laue case and substitute $\cos\Theta_B$ for γ_0 and γ_g. The position S on the exit surface of crystal B will be measured as the distance σ from an origin at the mid-point of R_1T_2. Then the relations between σ and the perpendiculars $\eta_1+\eta_2$, etc., are

$$\begin{aligned}\eta_1+\eta_2&=[\quad \sigma+(t+t_g)\tan\Theta_B]\cos\Theta_B\,,\\ \eta_1-\eta_2&=[-\sigma+(t-t_g)\tan\Theta_B]\cos\Theta_B\end{aligned}\tag{11 a}$$

and

$$\begin{aligned}\eta_1+\eta_3&=[\quad \sigma+(t-t_g)\tan\Theta_B]\cos\Theta_B\,,\\ \eta_1-\eta_3&=[-\sigma+(t+t_g)\tan\Theta_B]\cos\Theta_B\,.\end{aligned}\tag{11 b}$$

Combining Eq. (11) with Eq. (10), we obtain for the symmetrical Laue case

$$\begin{aligned}\Phi_{0g}^{11}(\sigma)=(i/16\pi)\,E_e(\chi_g/\chi_{\bar g})^{\frac12}(\beta/Kz_{B'})^{\frac12}\exp\{2\pi i\,\boldsymbol{g}\cdot\boldsymbol{r}_{B'}\}\exp\{i\,\delta_{BA}\}\\ \times\exp\{i(\tfrac12 K\chi_0 t\sec\Theta_B+Kz_{B'}-\pi/4)\;(t\sin\Theta_B)^{-\frac12}\}\,[1-(\sigma/t\tan\Theta_B)-(t_g/t)]\\ \times\{1-[(\sigma/t\tan\Theta_B)+(t_g/t)]^2\}^{-\frac14}\exp i\{\beta\,t\sin\Theta_B\{1-[(\sigma/t\tan\Theta_B)+(t_g/t)]^2\}^{\frac12}+\pi/4\}\end{aligned}\tag{12 a}$$

and

$$\begin{aligned}\Phi_{gg}^{11}(\sigma)=(i/16\pi)\,E_e(\chi_g/\chi_{\bar g})^{\frac12}(\beta/Kz_{B'})^{\frac12}\exp\{2\pi i\,\boldsymbol{g}\cdot\boldsymbol{r}_{B'}\}\\ \times\exp\{i(\tfrac12 K\chi_0 t\sec\Theta_B+Kz_{B'}-\pi/4)\;(t\sin\Theta_B)^{-\frac12}\}\\ \times[1+(\sigma/t\tan\Theta_B)-(t/t_g)]\;\{1-[(\sigma/t\tan\Theta_B)-(t_g/t)]^2\}^{-}\\ \times\exp i\{\beta\,t\sin\Theta_B\{1-[(\sigma/t\tan\Theta_B)-(t_g/t)]^2\}^{\frac12}+\pi/4\}\,.\end{aligned}\tag{12 b}$$

The required intensity field of the superposed beams is

$$I(\sigma)=|\Phi_{0g}^{11}(\sigma)+\Phi_{gg}^{11}(\sigma)|^2\,.\tag{13 a}$$

X-ray absorption will now be taken into account in the conventional way by replacing χ_0 and β by complex quantities: thus, $\chi_0=\chi_0'+i\chi_0''$ and $\beta=\beta'-i\beta''$. The connection between $K\chi_0''$ and the normal linear absorption coefficient μ_0 is $K\chi_0''=\mu_0$; whereas β'' is related to the Borrmann transmission and is given by

$$\beta''=KC[(\chi_g\chi_{\bar g})^{\frac12}]''\operatorname{cosec}2\Theta_B\,,$$

or more simply by

$$\beta''=KC\,|\chi_g''|\cos(\alpha_g''-\alpha_g')\operatorname{cosec}2\Theta_B$$

upon substituting $\chi_g'=-|\chi_g'|\exp\{i\alpha_g'\}$ and $\chi_g''=|\chi_g''|\exp\{i\alpha_g''\}$, and with Friedel's Law and the condition $|\chi_g''|/|\chi_g'|\ll1$ being satisfied. (Note that our representation of a plane wave as $\exp\{i\boldsymbol{K}\cdot\boldsymbol{r}\}$ makes χ_0'' positive, and that our above definition of α_g' identifies this angle with the conventional phase angle of the structure factor F_g'. The temperature factor will be deemed included in $|\chi_g''|$.)

The right-hand side of Eq. (13 a) can be simplified by introducing the parameter $p=\sigma/t\tan\Theta_B$, and by denoting t_g/t by q. In the present case p lies within the range $-1+q\leqq p\leqq 1-q$. Equation (13 a) thus becomes

$$\begin{aligned}I(\sigma)=D^2\exp\{-\mu_0 t\sec\Theta_B\}\;\{&[1-(p+q)]^2\,[1-(p+q)^2]^{-\frac12}\exp\{2\beta''t\sin\Theta_B\sqrt{1-(p+q)^2}\}\\ &+[1+(p-q)]^2\,[1-(p-q)^2]^{-\frac12}\exp\{2\beta''t\sin\Theta_B\sqrt{1-(p-q)^2}\}\\ &+2[(1-q)^2-p^2]\,[1-(p+q)^2]^{-\frac14}\,[1-(p-q)^2]^{-\frac14}\\ &\times\cos[(\beta' t\sin\Theta_B)\,(\sqrt{1-(p+q)^2}-\sqrt{1-(p-q)^2})+\delta_{BA}]\\ &\times\exp\{\beta''t\sin\Theta_B\,(\sqrt{1-(p+q)^2}+\sqrt{1-(p-q)^2})\}\}\,.\end{aligned}\tag{13 b}$$

The factor D^2 in Eq. (13 b) is

$$D^2=(1/16\pi)^2E_e^2(|\beta|/Kz_{B'})\,(1/t\sin\Theta_B)\,.$$

The argument of the cosine in Eq. (13 b) varies as p changes: thence arise the interference fringes of present concern. Prior to detailed discussion of the cosine function, a clearer display of its role may be achieved

by recasting Eq. (13 b) in the form

$$I(\sigma) = D^2 \exp\{-\mu_0 t \sec\Theta_B\}\ A \exp \bar{B}\{F \cosh U + G \sinh U + \cos[(\beta' t \sin\Theta_B)(\sqrt{1-(p+q)^2} - \sqrt{1-(p-q)^2}) + \delta_{BA}]\}. \quad (14)$$

In Eq. (14) the exponential factors of Eq. (13 b) have been re-grouped so that $\exp\{\bar{B}\}$ represents the mean Borrmann transmission of the rays reaching S, whereas U is a measure of the difference in Borrmann transmission enjoyed by the $\binom{11}{0\bar{g}}$ and $\binom{11}{g\bar{g}}$ rays: thus

$$\bar{B} = \beta'' t \sin\Theta_B (\sqrt{1-(p-q)^2} + \sqrt{1-(p+q)^2}) \quad (15\,a)$$

and

$$U = \beta'' t \sin\Theta_B (\sqrt{1-(p-q)^2} - \sqrt{1-(p+q)^2}). \quad (15\,b)$$

The coefficient A can be conveniently expressed in ascending powers of q,

$$A = 2(1-p^2)^{\frac{1}{2}}\left\{1 - \frac{2q}{(1-p^2)} + \frac{q^2}{(1-p^2)}\left[1 + \frac{1}{4}\frac{(2+p^2)}{(1-p^2)}\right]\right\}. \quad (16\,a)$$

Correspondingly, F and G may be written in series form as

$$F = (1+p^2)/(1-p^2) + 2p^2 q/(1+p)^2(1-p)^2 + 6p^2 q^2/(1+p)^3(1-p)^3 - \ldots \quad (16\,b)$$

and

$$G = 2p/(1-p^2) + pq(1+p^2)/(1+p)^2(1-p)^2 + 2p^2 q^2(1+3p^2)/(1+p)^3(1-p)^3 + \ldots. \quad (16\,c)$$

Representative maximum values attained by the smaller quantities in Eqs. (16) in actual experiments will be quoted below in Section 3. Note that as p tends to zero, F tends to unity, and G and U both tend to zero.

Consider now the cosine function in Equation (14). The difference term involving p and q which appears in its argument may be expanded as

$$[1-(p+q)^2]^{\frac{1}{2}} - [1-(p-q)^2]^{\frac{1}{2}} = -2pq/(1-p^2)^{\frac{1}{2}} - q^3[p/(1-p^2)^{3/2} + p^3/(1-p^2)^{5/2}] + \ldots. \quad (17)$$

If only the first term of the series on the right-hand side of Eq. (17) is included, then

$$\cos[(\beta' t \sin\Theta_B)(\sqrt{1-(p+q)^2} - \sqrt{1-(p-q)^2}) + \delta_{BA}] \approx \cos[-2pq(1-p^2)^{-\frac{1}{2}}(\beta' t \sin\Theta_B) + \delta_{BA}]. \quad (18)$$

The right-hand side of Eq. (18) may be written

$$\cos[(-2\pi\sigma t_g/\Lambda_g^c t \tan\Theta_B)(1-\sigma^2/t^2\tan^2\Theta_B)^{-\frac{1}{2}} + \delta_{BA}]$$

upon reverting to σ as variable and substituting $\beta' \sin\Theta_B = (\pi/\Lambda_g^c)$ where Λ_g^c is the Pendellösung fringe distance along the Bragg plane. Maxima of the cosine function occur at positions $\sigma(k)$ given by

$$\sigma(k) = (k-e)(\Lambda_g^c t_g^{-1} t \tan\Theta_B)[1 + (\Lambda_g^c t_g^{-1})^2 (k-e)^2]^{-\frac{1}{2}} \quad (19)$$

in which k is an integer and e is the fraction defined by $2\pi e = \delta_{BA}$ modulo 2π. Equation (19) differs from the analogous equation derived by Authier et al.[7] only by the inclusion of the phase shift due to δ_{BA}. This inclusion follows naturally from the present stricter treatment. However, the approximation made in deriving Eq. (18) from Eq. (17) requires examination; but before this is done two other factors should be considered, and these are dealt with in the following Sections 2.4 and 2.5.

2.4. Effect of Deviation from the Symmetrical Laue Geometry

Let there be a deviation from the symmetrical Laue condition by the small angle ω, giving

$\gamma_g = \cos(\Theta_B + \omega)$ and $\gamma_0 = \cos(\Theta_B - \omega)$. Neglecting terms in ω^2, we find

$$(\eta_1^2 - \eta_2^2)^{\frac{1}{2}} = t \sin\Theta_B[(1-p^2)^{\frac{1}{2}} - pq(1-p^2)^{-\frac{1}{2}} + \omega(1-p^2)^{-\frac{1}{2}}(\tan\Theta_B + 2p\,\mathrm{cosec}\,2\Theta_B - p^2\tan\Theta_B)],$$

$$(\eta_1^2 - \eta_3^2)^{\frac{1}{2}} = t \sin\Theta_B[(1-p^2)^{\frac{1}{2}} + pq(1-p^2)^{-\frac{1}{2}} + \omega(1-p^2)^{-\frac{1}{2}}(\tan\Theta_B + 2p\,\mathrm{cosec}\,2\Theta_B - p^2\tan\Theta_B)]$$

and

$$\tfrac{1}{2} K \chi_0 \gamma_g^{-1}(1-b^{-1})\, t_g = K \chi_0 t_g \omega \tan\Theta_B \sec\Theta_B.$$

Using these equations in the procedure previously adopted from Eqs. (10) onwards for deriving the oscillatory term in the expression for $I(\sigma)$ we find the right-hand side of Eq. (18) replaced by

$$\cos[-2\,p\,q(1-p^2)^{-\frac{1}{2}}(\beta' t \sin\Theta_B) + \delta_{BA} + K\chi_0 t_g \omega \tan\Theta_B \sec\Theta_B] .$$

[Note that the origin of σ is now located at the intersection of the line $x = t\sin(\Theta_B - \omega) + \alpha t_g$ with the exit surface of crystal B.] Thus we see that a small departure from the symmetrical Laue geometry introduces a constant phase shift in the fringe system.

Taking $K \approx 2\pi \times 10^8\,\mathrm{cm}^{-1}$, $\chi_0 \approx 10^{-5}$, $t_g \approx 5 \times 10^{-2}$ cm, $\Theta_B \approx 10^\circ$ and $\omega \approx \pm 2 \times 10^{-2}$ radians, the fringe shift is about $\pm\frac{1}{3}\pi$. For practical purposes this shift may be absorbed into δ_{BA}.

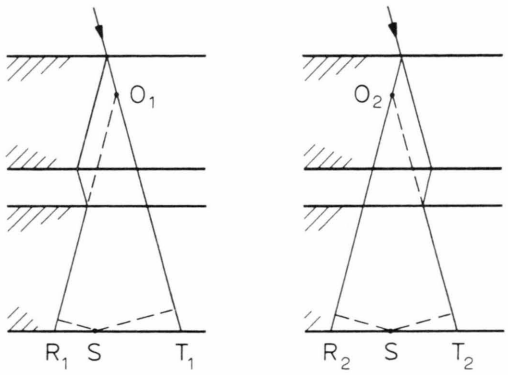

Fig. 4. The location of S (position vector $\boldsymbol{r}_{B'}$) with respect to (a) the region $R_1 T_1$ covered by wave field Φ_{0g}^{11} and, (b) the region $R_2 T_2$ covered by wave field Φ_{gg}^{11}. Drawn for symmetrical Laue case. In general case, perpendicular distances are: from S to $O_1 T_1$, $\eta_1+\eta_2$; from S to $O_1 R_1$, $(\eta_1-\eta_2)b^{-1}$; from S to $O_2 T_2$, $(\eta_1-\eta_3$; and from S to $O_2 R_2$, $(\eta_1-\eta_3)b^{-1}$.

2.5. *Effect of Incident Wavefront Curvature*

In the derivation of Eqs. (9) the incident wave vector $\boldsymbol{K}_e$ was represented by the components $K\hat{\boldsymbol{z}} + K_x\hat{\boldsymbol{x}}$, where $\hat{\boldsymbol{x}}$ and $\hat{\boldsymbol{z}}$ are unit vectors in the directions of the x and z axes (see Figure 3). The assumption that K_z is equal to K is equivalent to replacing the spheres of radius $|\boldsymbol{K}| = K$ by tangent planes at their intersection at the Laue point [9, 10]. The next step of approximation [11] is to represent $\boldsymbol{K}_e$ by $[K - \frac{1}{2}(K_x^2/K)]\,\hat{\boldsymbol{z}} + K\hat{\boldsymbol{x}}$. When this is done, account may be taken of the initial phase difference of the waves which recombine at S after passing through the crystals in the $\binom{11}{0g}$ and $\binom{11}{gg}$ states respectively. As Kato [11] has pointed out, introduction of the $(\frac{1}{2}K_x^2/K)$ term has insignificant effects on the Pendellösung fringe pattern of an undistorted crystal since the branch (1) and branch (2) waves which propagate in a common direction can still be specified to a good approximation by conjugate tie points on a hyperbolic dispersion surface, i. e. by points corresponding to $\pm K_x$. On the other hand in experiments such as those now under discussion, when interference is observed between rays with differing values of $|K_x|$, the effects of their respective initial phases may be significant. If the previously used findings of the stationary condition

$[s] = \beta'\eta_2(\eta_1^2 - \eta_2^2)^{-\frac{1}{2}}$ for the Φ_{0g}^{11} wave

and $[s] = \beta'\eta_3(\eta_1^2 - \eta_3^2)^{-\frac{1}{2}}$ for the Φ_{gg}^{11} wave

are adopted, we find an additional phase term in the Φ_{0g}^{11} wave given by

$$\exp\{-i[\tfrac{1}{2}K^{-1}z_{B'}(\beta'\eta_2(\eta_1^2-\eta_2^2)^{-\frac{1}{2}} + \tfrac{1}{2}K\chi_0 \operatorname{cosec} 2\Theta_B\ (b^{-1}-1))^2]\}$$

and a corresponding additional phase term in the Φ_{gg}^{11} wave given by

$$\exp\{-i[\tfrac{1}{2}K^{-1}z_{B'}(\beta'\eta_3(\eta_1^2-\eta_3^2)^{-\frac{1}{2}} + \tfrac{1}{2}K\chi_0 \operatorname{cosec} 2\Theta_B\ (b^{-1}-1))^2]\} .$$

Therefore, in the symmetrical Laue case, the term

$$-\tfrac{1}{2}K^{-1}z_{B'}(\beta')^2\{(p+q)^2[1-(p+q)^2]^{-1} - (p-q)^2[1-(p-q)^2]^{-1}\}$$

should be added to the argument of the cosine term in Equation (14). To the same degree of approximation as was introduced in the right-hand side of Eq. (18), this addition, the curvature term, $c(p)$, may be written as

$$c(p) = -2\,p\,q(1-p^2)^{-1}K^{-1}z_{B'}(\beta')^2. \qquad (20)$$

Strictly, a small perturbation term caused by the factor $\frac{1}{2}K_x^2 z_{B'}/K$ should be included in the stationary values $[s]$. Its effect on ray trajectories can, however, be seen without calculation. The curvature of the $\boldsymbol{K}$ spheres is of opposite sign to that of the branch (1) hyperbola. Hence, as the mean value of $|p|$ for the waves recombining at S increases, they will need to have a greater spacing between their tie-points on the branch (1) surface (i. e. a greater difference in K_x values) than would be predicted with the tangent-plane approximation. Therefore, for branch (1) waves, the perturbation will increase the magnitude of $c(p)$. [Its effect would be opposite if interference between branch (2) waves were being considered.]

3. Discussion

We will confine our discussion to some of the problems encountered in exploiting "gap-fringes" for precision absolute measurements of structure factors, as has been done by Hart and co-workers [1, 2].

Firstly, we must remember the assumption that only interference between Φ_{0g}^{11} and Φ_{gg}^{11} waves need be considered. Now as long as $t_A \approx t_B$ and the ratio q is small, rays which travel as a branch (1) Bloch wave in one crystal and as a branch (2) wave in the other are all focussed into a narrow band of width $2\,t_g \tan\Theta_B$ centred at the origin of σ. Provided that this band is sufficiently narrow compared with the range of σ within which measurable fringes occur, the presence of these "jumped" waves need not preclude use of the gap fringe system for accurate structure factor determination, though the most central fringes would have to be alloted reduced weight when fitting the observed fringe pattern to a computed pattern. Note that the appearance of a modulation in gap-fringe visibility near $\sigma = 0$ when the crystal is twisted (and when in consequence a sloping fringe pattern is produced) provides a quite sensitive test for the presence of jumped waves with significant amplitudes (as seen, for example, in the patterns shown in Figure 1). On the other hand, the Φ_{0g}^{22} and Φ_{gg}^{22} waves are everywhere superimposed on the Φ_{0g}^{11} and Φ_{gg}^{11} waves, and the overall appearance of the gap-fringe pattern provides no obvious indication whether they are significant or not. Whereas $|\Phi_{0g}^{22}|^2$ may indeed be negligible compared with $|\Phi_{0g}^{11}|^2$, say, it must be borne in mind that the interference terms between these waves will have absolute strengths closely similar to the strength of Pendellösung interference in a single crystal of thickness t. In fact, the interference pattern of the four waves $\Phi_{0g}^{11}(\sigma)$, $\Phi_{0g}^{22}(\sigma)$, $\Phi_{gg}^{11}(\sigma)$ and $\Phi_{gg}^{22}(\sigma)$ has some interesting properties which it is hoped to describe elsewhere (Tanemura and Lang, in preparation).

With crystals prepared as carefully as those Hart and co-workers used [1, 2], no fear need be entertained that any departure from the exact symmetrical Laue condition was greater than could adequately be treated by the analysis in Section 2.4. As already mentioned, a fractional fringe order shift caused by deviation from symmetrical Laue geometry would not be separable from the residuum e resulting from a moiré-type shift due to δ_{BA}. Possibly it might be worthwhile in precision measurements to fashion the specimen so that a small twist moiré component could be deliberately introduced, and the photometry of the pattern performed only at levels where e was zero as shown by exact mirror symmetry of the pattern about a central maximum. Such a procedure would facilitate matching the photometric profiles with computed ones.

We turn next to consider the approximation whereby the right-hand side of Eq. (18) was derived. When we include the term $-p\,q^3[1-p^2]^{-3/2}$ which appears on the right-hand side of Eq. (17), the resulting modification of the right hand side of Eq. (18) is

$$\cos\{-2\,p\,q(1-p^2)^{-\frac{1}{2}}(\beta' t \sin\Theta_B) \cdot [1+\tfrac{1}{2}q^2(1-p^2)^{-1}] + \delta_{BA}\}.$$

In the reported experiments on silicon [1], the mean value of q was $1/15$, so $\frac{1}{2}q^2 \approx 2.2\times10^{-3}$. In the recent work on germanium [2] q ranged from $1/13$ to $1/16$, giving values of $\frac{1}{2}q^2$ ranging from 3.0×10^{-3} to 1.9×10^{-3}.

Finally, we consider the importance of wave front curvature under the experimental conditions used in observing gap fringes in the case of silicon with MoKα radiation [1] and in the case of germanium with AgKα radiation [2], taking values of $z_{B'}$ used in the experiments. The functional form of the dependence of the curvature term $c(p)$ on p, as shown in Eq. (20), is sufficiently similar to that of the phase difference which produces the gap fringes to permit $c(p)$ to be included as a small additional factor in the expression for the gap fringe phase. Thus the argument of the cosine term should be

$$-2\,p\,q(1-p^2)^{-\frac{1}{2}}(\beta' t\sin\Theta_B)[1+\tfrac{1}{2}q^2(1-p^2)^{-1} + \beta' z_{B'} K^{-1} t^{-1} \operatorname{cosec}\Theta_B (1-p^2)^{-\frac{1}{2}}] + \delta_{BA}$$

rather than as written on the right-hand side of Eq. (18), which latter expression was used in interpreting the experiments [1, 2]. Inserting the values of $z_{B'}$ employed, $z_{B'} = 72$ cm in the work on silicon and $z_{B'} = 66$ cm in the work on germanium (Hart, private communication), we find, with the average values of t used, that

$$\beta' z_{B'} K^{-1} t^{-1} \operatorname{cosec}\Theta_B = 2.8\times10^{-3}$$

in the silicon experiments, and

$$\beta' z_{B'} K^{-1} t^{-1} \operatorname{cosec}\Theta_B = 10.4\times10^{-3}$$

in the germanium experiments. Thus, for small p and the average value of t, allowance for both the

term $\frac{1}{2} q^2$ discussed above and for the incident wavefront curvature multiplies the argument of the cosine term by a factor which amounts to

$$(1+2.2\times10^{-3}) + (2.8\times10^{-3}) = 1+5\times10^{-3}$$

in the case of silicon, and

$$(1+2.5\times10^{-3}) + (10.4\times10^{-3}) = 1+13\times10^{-3}$$

in the case of germanium. Hence these revisions of the formulae which have been accepted as the basis for interpreting the fringe spacing measurements imply a reduction in the calculated central fringe spacing by 0.5% in the case of silicon, and by 1.3% in the case of germanium. Such changes are significant when compared with the standard errors, $\pm 0.2\%$ for silicon and $\pm \frac{1}{3}\%$ for germanium, reported in the structure factor determinations [1, 2].

Acknowledgment

One of the authors (S. T.) wishes to thank the Royal Society Paul Instrument Fund and the U. K. Science Research Council for financial support.

[1] M. Hart and A. D. Milne, Acta Cryst. **A 26**, 223 [1970].
[2] J. F. C. Baker, M. Hart, and J. Helliar, Z. Naturforsch. **28 a**, ■■ [1973].
[3] A. R. Lang and V. F. Miuscov, Appl. Phys. Lett. **7**, 214 [1965].
[4] J. T. Hagan, M. Sc. Thesis, Bristol 1969.
[5] A. D. Milne, M. Sc. Thesis, Bristol 1966.
[6] A. J. Durelli and V. J. Sparks, Moiré Analysis of Strain, Prentice Hall, Englewood Cliffs, N. J., U.S.A. 1970.
[7] A. Authier, A. D. Milne, and M. Sauvage, Phys. Stat. Sol. **26**, 469 [1968].
[8] N. Kato, K. Usami, and T. Katagawa, Advances in X-ray Analysis, Plenum Press, New York, **10**, 46 [1967].
[9] N. Kato, Acta Cryst. **14**, 526, 627 [1961].
[10] N. Kato, J. Appl. Phys. **39**, 2225, 2231 [1968].
[11] N. Kato, Acta Geologica et Geographica Universitatis Comenianae, Bratislava, Geologica Nr. **14**, 43 [1968].

Dislocation-free Silver Single Crystals Grown by the Czochralski Method

B. K. Tanner

Department of Metallurgy, Oxford University, Parks Road, Oxford, England

(Z. Naturforsch. **28 a**, 676–678 [1973]; received 22 January 1973)

Dedicated to Professor G. Borrmann on the occasion of his 65th birthday

Single crystals of pure silver have been grown by the Czochralski technique and Borrmann X-ray topography has been used to study the perfection of the as-grown crystals. Conditions have been found under which dislocation-free growth takes place and crystals of about 1 cm length and 1 mm diameter have been grown free from dislocations.

1. Introduction

While large, dislocation-free crystals of semi-conducting materials have been available for many years [1, 2], it is only recently that relatively large volume metal single crystals have been grown free from dislocations. Following earlier work on copper, which showed that crystals grown by the Czochralski technique had lower dislocation densities than similar crystals grown by the Bridgman method [3], both Fehmer and Uelhoff [4], and Sworn and Brown [5] used the Czochralski method to pull dislocation-free copper crystals. Both pairs of authors took great care to minimise thermal gradients, the only major difference in technique being that while Sworn and Brown grew their crystals under an argon atmosphere, Fehmer and Uelhoff grew crystals under high vacuum. In the latter situation, the elimination of heat loss by convection enables much larger diameter crystals to be grown dislocation-free under otherwise similar conditions.

Borrmann X-ray topography was used by the present author [6] to establish the perfection of copper crystals grown by the method of Sworn and Brown. The technique of anomalous transmission X-ray topography, first employed to reveal dislocations by Borrmann et al. [7], is ideally suited to studying nearly perfect copper (and silver) crystals of about 1 mm thickness. In this situation, for Mo Kα radiation, $\mu t \sim 40$ and unless the crystal is very nearly perfect, no transmitted intensity will be detected.

Reprint requests to Dr. B. K. Tanner, Department of Metallurgy, University of Oxford, Parks Road, *Oxford*, England.